

PCCP

Accepted Manuscript



This is an *Accepted Manuscript*, which has been through the Royal Society of Chemistry peer review process and has been accepted for publication.

Accepted Manuscripts are published online shortly after acceptance, before technical editing, formatting and proof reading. Using this free service, authors can make their results available to the community, in citable form, before we publish the edited article. We will replace this *Accepted Manuscript* with the edited and formatted *Advance Article* as soon as it is available.

You can find more information about *Accepted Manuscripts* in the [Information for Authors](#).

Please note that technical editing may introduce minor changes to the text and/or graphics, which may alter content. The journal's standard [Terms & Conditions](#) and the [Ethical guidelines](#) still apply. In no event shall the Royal Society of Chemistry be held responsible for any errors or omissions in this *Accepted Manuscript* or any consequences arising from the use of any information it contains.

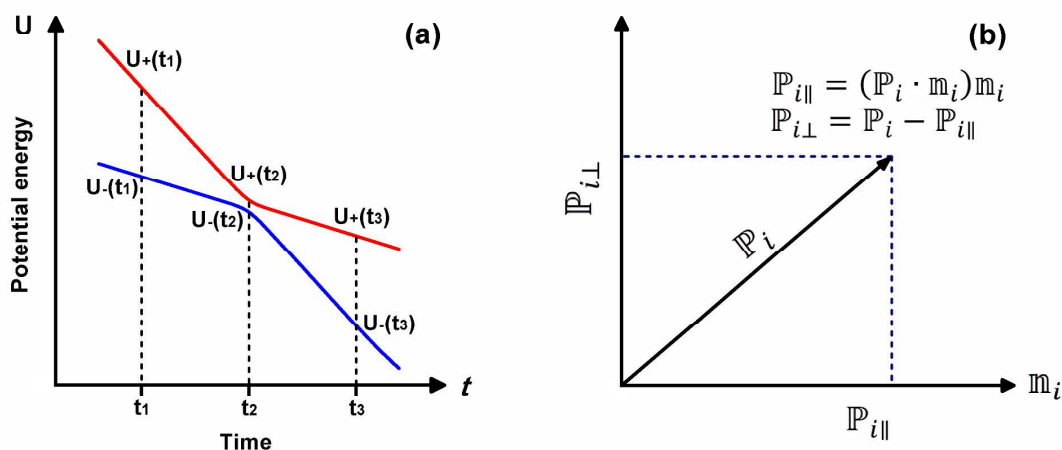


Fig. 1. Hopping scheme along trajectory. (a) Hopping point (t_2) at minimum energy separation between two adiabatic potential energy surfaces. (b) Classical momentum decomposition according to hopping direction n_i .

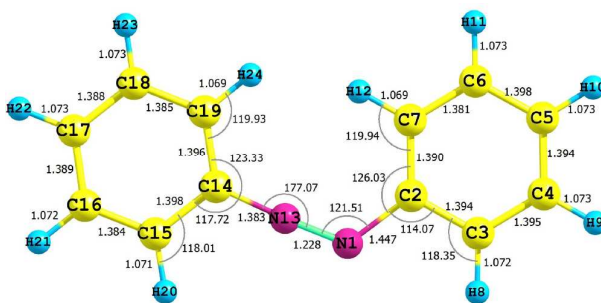


Fig. 2. Atom numbering (geometry of TS-planar-inv in S_0 state).

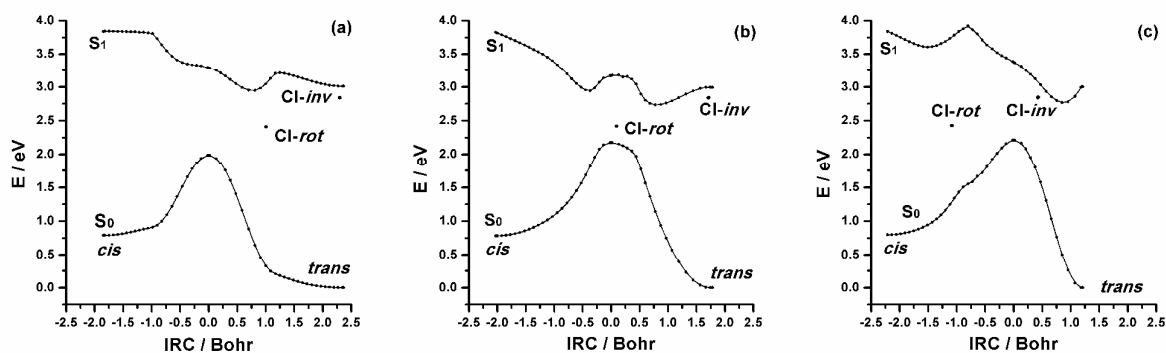


Fig. 3. Potential energy profiles for three transition states in S_0 state along intrinsic reaction coordinate. (a) inversion-assisted rotation. (b) rotation and (c) inversion. The conical intersections between S_0 and S_1 states, CI-rot and CI-inv, are also plotted for comparison.

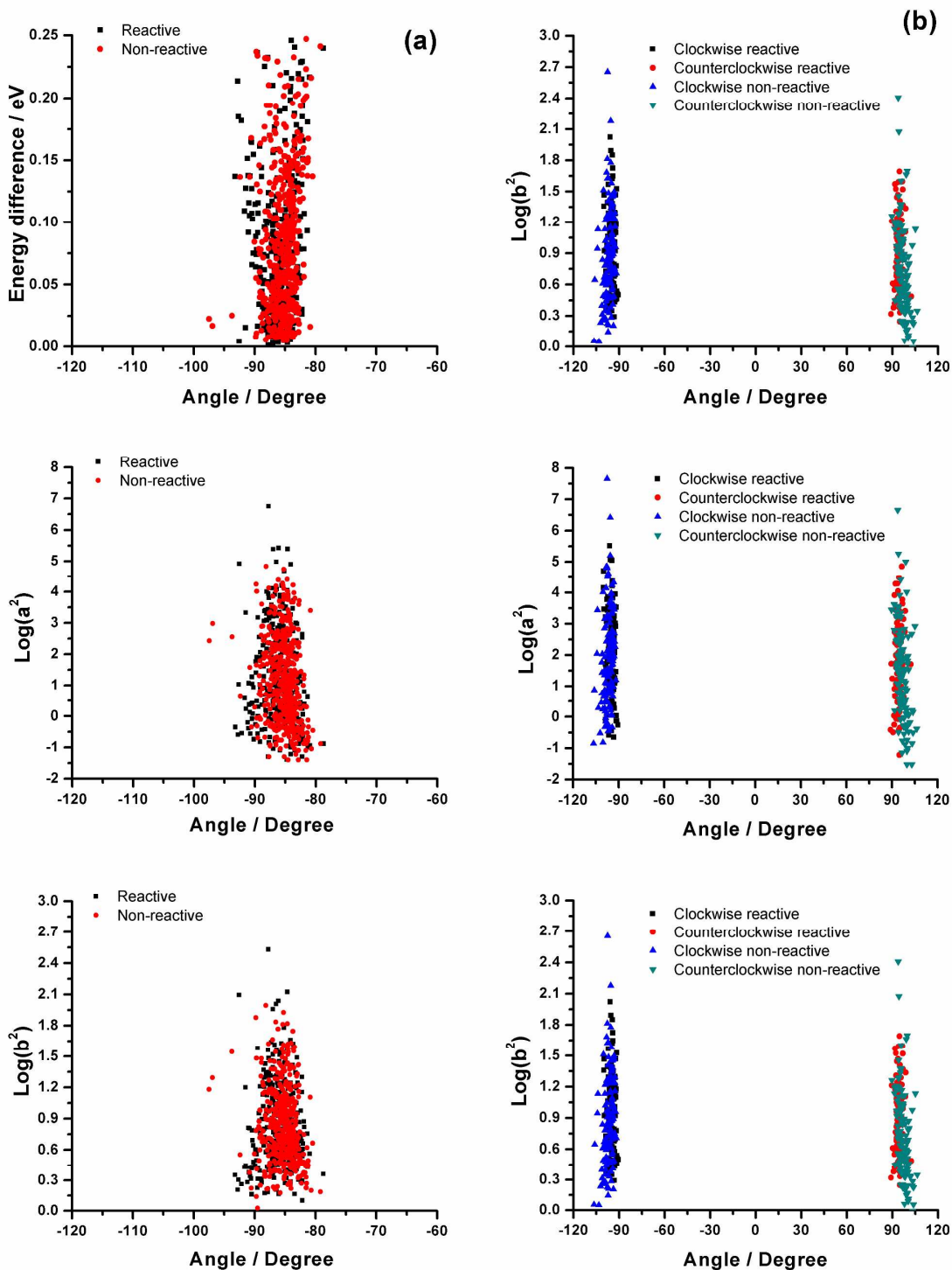


Fig. 4. The distribution of successful hopping points in terms of CNNC dihedral angle. (a) The first panel is for energy gaps, second panel is for effective coupling parameter, and third panel is for effective collision energy in the case of cis-to-trans. (b) The same as (a) but in case of trans-to-cis.

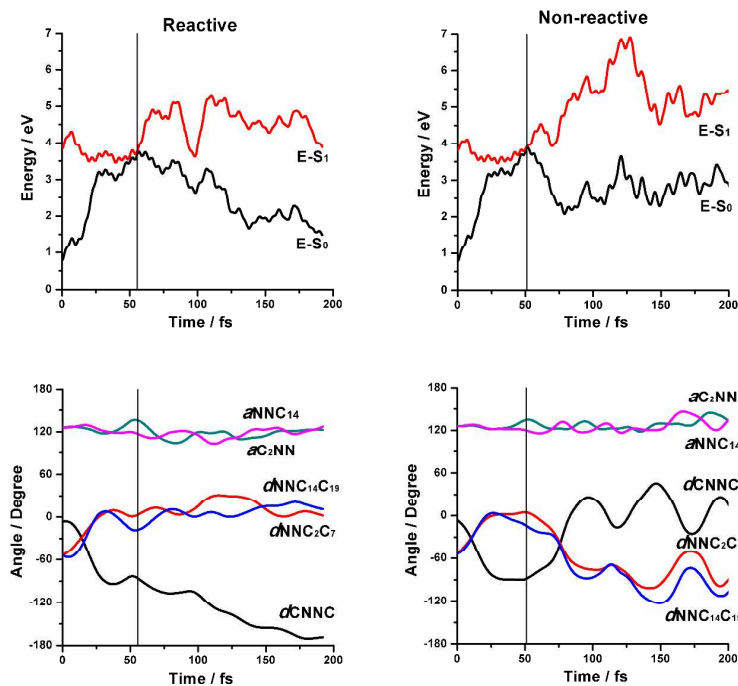


Fig. 5. Potential energies and the five important angles evolve along trajectory starting from cis-azobenzene. A typical reactive (left panel) with $a^2 = 14.79$ and $b^2 = 3.52$ at hopping point and a typical non-reactive (right panel) trajectory with $a^2 = 75.35$ and $b^2 = 4.82$.

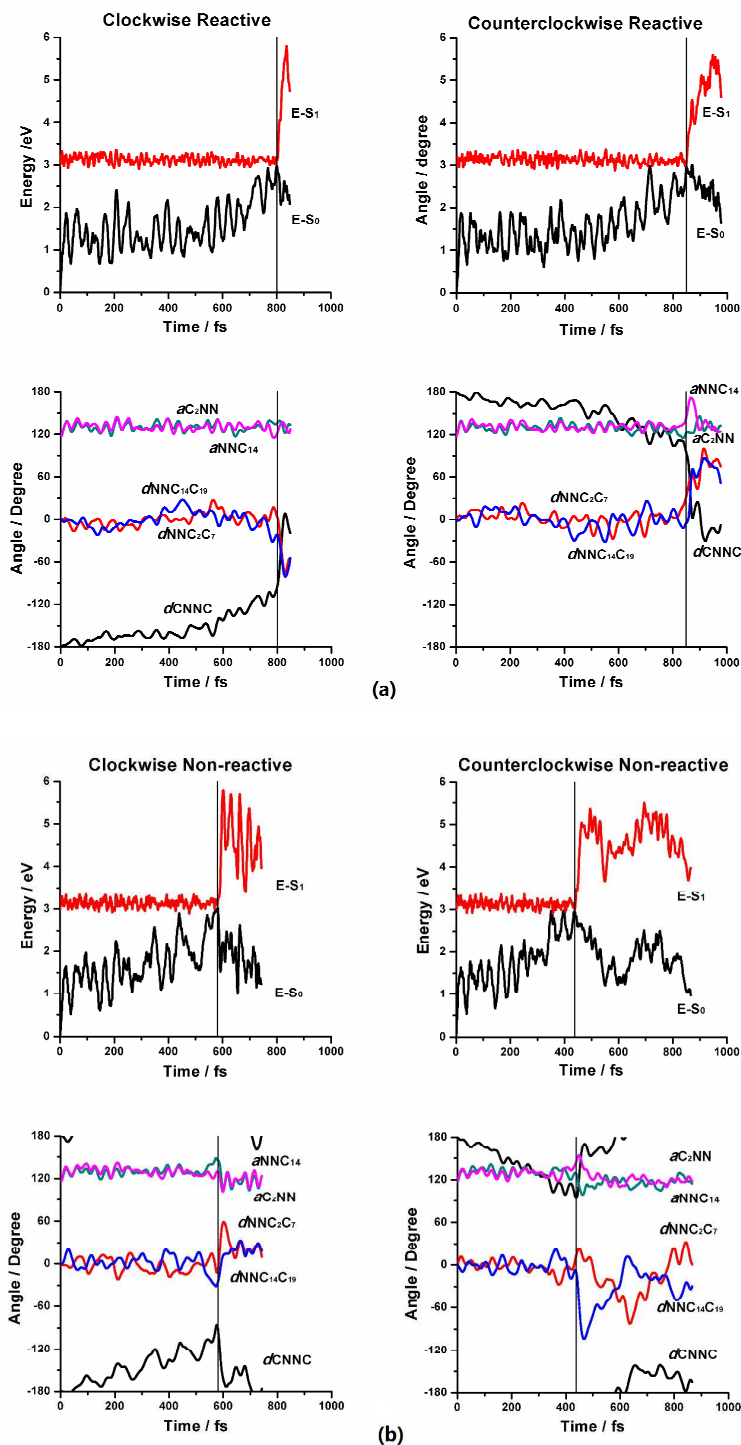


Fig. 6. Potential energies and the five important angles evolve along trajectory starting from trans-azobenzene. (a) Typical reactive trajectories; clockwise one (left panel) with $a^2 = 0.22$ and $b^2 = 1.95$ and counterclockwise one (right panel) with $a^2 = 35.84$ and $b^2 = 4.26$. (b) Typical non-reactive trajectories; clockwise one (left panel) with $a^2 = 9.50$ and $b^2 = 3.07$ and counterclockwise one (right panel) with $a^2 = 48.17$ and $b^2 = 6.65$.

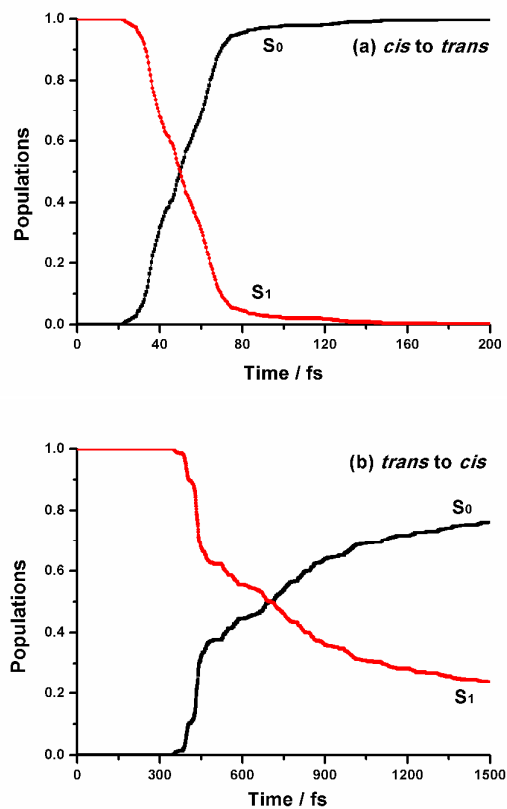


Fig. 7. Average population distribution in S_1 and S_0 states as function of time. (a) Cis-to-trans estimated from 800 trajectories. (b) Trans-to-cis estimated from 600 trajectories.

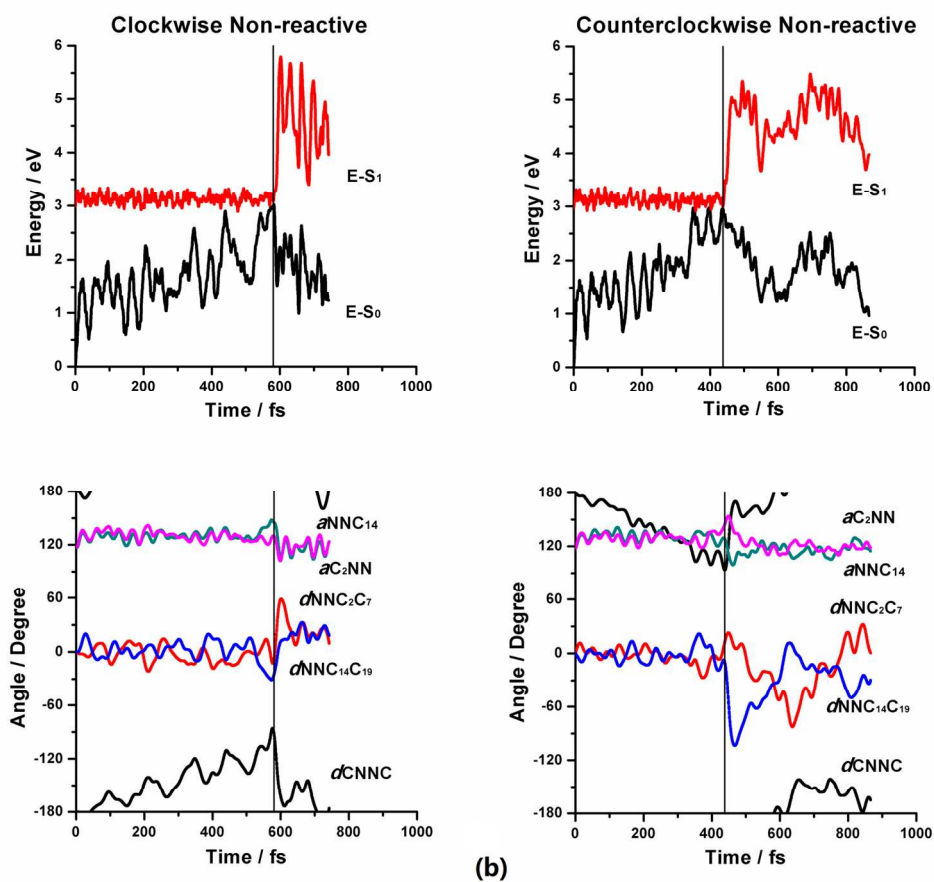


Figure 6b
152x136mm (300 x 300 DPI)

Prepared for publication in Physical Chemistry Chemical Physics

August 6, 2014

Revised September 21, 2014

Trajectory based nonadiabatic molecular dynamics without calculating nonadiabatic coupling in the avoided crossing case: Trans \leftrightarrow cis photoisomerization in azobenzene

Le Yu¹, Chao Xu^{1,2}, Yibo Lei³, Chaoyuan Zhu^{1*} and Zhenyi Wen³

¹*Institute of Molecular Science, Department of Applied Chemistry, and Center for Interdisciplinary Molecular Science, National Chiao-Tung University, Hsinchu 300, Taiwan*

²*Department of Chemistry, Beijing Normal University, Beijing 100875, PR China*

³*Institute of Modern Physics, Northwest University, Xi'an, 710069, PR China*

Abstract. We develop a novel method to simulate analytical nonadiabatic switching probability based on effective coupling and effective collision energy by only using electronic adiabatic potential energy surfaces and its gradients in the case of avoided crossing type of nonadiabatic transitions. Besides, the present method can keep the same time step for computing both on-the-fly trajectory and nonadiabatic transitions accurately. The present method is most useful for localized nonadiabatic transitions induced by conical intersection. We employ the on-the-fly surface hopping algorithm with ab initio quantum

*To whom correspondence should be addressed. Email: cyzhu@mail.nctu.edu.tw

chemistry calculation to demonstrate dynamic simulation for photoisomerization in azobenzene. Simulated quantum yield and lifetime converge to 0.39 and 53 femtosecond (0.33 and 0.81 picosecond) for cis-to-trans (trans-to-cis) photoisomerization with up to 800 (600) sampling trajectories. The present results agree well with experiment results as well as results simulated with use of nonadiabatic coupling within Tully's fewest switching method. The present trajectory based nonadiabatic molecular dynamics free from nonadiabatic coupling greatly enhances simulation power of molecular dynamic for large complex chemical systems.

1. Introduction

Trajectory based non-Born-Oppenheimer molecular dynamics, one of the most important tool to study of photophysical and photochemical processes for large complex chemical systems [1], extends classical trajectory of nuclear motion from electronic ground-state potential energy surface (PES) to electronic excited-state PES [2]. It is nonadiabatic coupling between two electronic states that drives classical trajectory switching from one electronic state to another. Trajectory surface hopping (TSH) method is stochastic method which attempts to make the electronic probability distribution averaged over an ensemble of trajectories equal to the probability distribution computed from the electronic density matrix. The TSH methods mostly differ in computing nonadiabatic switch probability which governs trajectory hopping from one electronic potential energy surface to another. Tully's fewest switches (TFS) trajectory surface hopping [3] provides one of the most successful methods to calculate this switching probability which is extended to nonadiabatic Car-Parrinello molecular dynamics [4] and nonadiabatic molecular dynamics with time-dependent density functional methods [5,6]. This switching probability is solved by integrating the first-order coupled time-dependent Schrödinger equations involving coupling term $\sum_{i=1}^N \dot{\mathbf{R}}_i \cdot \mathbf{d}_{12}^i$ (N is number of nuclei in molecule) in which $\dot{\mathbf{R}}_i$ is velocity of classical nuclei and \mathbf{d}_{12}^i is nonadiabatic coupling vector between two electronic states. Based on Landau-Zener two-state linear curve crossing model in which two linear diabatic potential energy curves and constant diabatic coupling are assumed at avoided crossing point, this switching probability has been formulated in terms of two unitless parameters, namely effective coupling and effective collision energy [7],

$$a^2 = \frac{\hbar^2 \sqrt{|F_2 F_1|} |F_2 - F_1|}{2\mu (2V_{12})^3} \quad (1)$$

and

$$b^2 = (E_t - E_x) \frac{|F_2 - F_1|}{\sqrt{|F_2 F_1|} (2V_{12})} \quad (2)$$

in which F_1 and F_2 are forces on two diabatic potential energy surfaces, V_{12} is diabatic coupling, μ is reduced mass of diatomic molecule, E_x is energy at crossing point and E_t (see Eq. (15)) is potential energy plus kinetic energy component in direction of nonadiabtic coupling vector. Based on these two unitless parameters, Zhu and Nakamura [8, 9] developed improved Landau-Zener formula for switching probability valid up to nonadiabtic transition region $b^2 \rightarrow 0$,

$$p = \exp \left[-\frac{\pi}{4\sqrt{a^2}} \sqrt{\frac{2}{b^2 + \sqrt{|b^4 \pm 1|}}} \right] \quad (3)$$

where + (-) stands for $F_1 F_2 > 0$ ($F_1 F_2 < 0$). The fewest switching probability is a local nonadiabatic transition probability calculated at each integration time step along a trajectory and in principle the trajectory can make an attempted hop anytime. On the other hand, the analytical switching probability in Eq. (3) is a global switching probability calculated at an avoided crossing point and it represents an averaged nonadiabatic transition probability along a trajectory. The trajectory surface hopping is actually carried out when this switching probability is greater than a uniform random number generated between 0 and 1. For system where nonadiabatic transitions occur dominantly at avoided crossing zones, two switching probabilities should lead to the same results. Actually, this analytical switching probability has been applied to the charge transfer reaction in the DH_2^+ system, and calculated cumulative

reaction probability and cross section are in good agreement with exact quantum mechanical calculations [10, 11]. However, it requires predetermining seam surface between two adiabatic potential energy surfaces instead of calculating nonadiabatic coupling vector. It is hard to apply this analytical switching probability to more than three-atom system due to difficulty of searching seam surfaces. By approximately estimating direction of nonadiabatic coupling vector, this switching probability has been applied to large systems where nonadiabatic transitions occur at localized conical intersection zones and it works well in comparison with experimental results; these were demonstrated in dihydrodibenzodiazocine photoisomerization [12] and on-the-fly nonadiabatic dynamics for the Schiff base of retinal [13]. Either predetermining seam surfaces or calculating nonadiabatic coupling vector restricts this analytical switching probability applied to large complex chemical and physical systems.

Here, we report a novel approach to generalize two parameters in Eqs. (1) and (2) along time-dependent classical trajectory based on only adiabatic potential energy surfaces and its gradients in the case that nonadiabatic transitions take place in avoided crossing zones. This makes the present method almost as simple as molecular dynamics on a single potential energy surface.

Nonadiabatic transitions through conical intersections play a significant role in many photochemical and photophysical processes [14]. Conical intersections exhibit localized characterization of nonadiabatic transitions, so that simulated trajectory may make surface hopping mostly appeared in the local region of avoided crossing zones. This makes ideal case to demonstrate trajectory based nonadiabatic molecular dynamics working with the analytical switching probability. There are many examples of photochemical isomerisations to involve conical intersections, and cis-to-trans and trans-to-cis azobenzene photoisomerization as a

prototype has been extensively studied both theoretically [15-22] and experimentally [23 and references therein]. Especially, it is worth mentioning that without calculating nonadiabatic coupling vector the switching probability $p = \kappa \exp[-\chi|\Delta V_{12}|]$ has been applied to study azobenzene photoisomerization [21, 22] in which κ and χ are fitting parameters. It is interesting to compare with the present form in Eq. (3) that takes form of $p \propto \exp[-\chi(\Delta V_{12})^2]$.

We employ on-the-fly trajectory surface hopping algorithm to study both cis-to-trans and trans-to-cis azobenzene photoisomerization. Adiabatic ground-state and the first excited-state potential energy surfaces and its gradients are calculated by state-averaged complete active space self-consistent field (SA-CASSCF) method with basis set 6-31G. The analytical switching probability is calculated on the fly along trajectory. We report simulated quantum yields and lifetimes for cis-to-trans with 800 sampling trajectories and for trans-to-cis with 600 sampling trajectories. We make an extensive comparison with the previous calculations based on TFS nonadiabatic switching probability.

The rest of this paper is organized as follows: Section 2 introduces the present algorithm how to generalize multidimensional form of the effective coupling and the effective collision energy as well as hopping direction only based on adiabatic potential energy surfaces and its gradients. Section 3 applies the present method to photoisomerization in azobenzene and shows why the SA2-CAS(6,6)/6-31G method is adequate for running on-the-fly nonadiabatic molecular dynamics for azobenzene. Section 4 present extensive comparisons with results calculated by Tully's fewest switching probability and by the energy-gap switching probability. Concluding remarks are mentioned in Section 5.

2. The new algorithm of diabaticization at avoided crossing zones

The nuclear coordinates and velocities in Cartesian coordinates are propagated along on-the-fly classical trajectories by numerically integrating the Newtonian equation of motion with the velocity-Verlet method [24]. From three consecutive time steps shown in Fig.1 (a) where the minimum adiabatic potential gap is assumed to be detected, we convert multidimensional forces into one-dimensional forces in Eqs.(1) and (2) along a trajectory,

$$\frac{|F_2 - F_1|}{\sqrt{\mu}} = \sqrt{\sum_{i=1}^N \frac{1}{m_i} \sum_{\alpha=x,y,z} (F_2^{i\alpha} - F_1^{i\alpha})^2} \quad , \quad (4)$$

and

$$\frac{\sqrt{|F_2 F_1|}}{\sqrt{\mu}} = \sqrt{\sum_{i=1}^N \frac{1}{m_i} \sum_{\alpha=x,y,z} F_2^{i\alpha} F_1^{i\alpha}} \quad (5)$$

where N is number of nuclei in molecule with the mass m_i ($i=1,2,\dots,N$), and multidimensional diabatic forces are given as

$$F_1^{i\alpha} = -\frac{\partial V_1}{\partial R_{i\alpha}} \quad \text{and} \quad F_2^{i\alpha} = -\frac{\partial V_2}{\partial R_{i\alpha}} \quad (6)$$

in which $R_{i\alpha}$ stands for x , y , and z component of Cartesian coordinates for the i -th nucleus. It is easy to prove that Eqs. (4) and (5) go back original form if diatomic molecule is applied. In the case of a conical intersection, the regularized diabatic states [25] can be defined by which we could generalize one-dimensional Landau-Zener avoided crossing along a curved coordinate of a trajectory in the form of Eq. (4) and detailed derivation is given in appendix A.

Next we generalize diabatic forces in Eq. (6) from two adiabatic potential energy gradients along a trajectory, and we simply make one linear connection of upper adiabatic force at t_1 with lower adiabatic force at t_3 , and another linear connection of lower adiabatic force at t_1 with upper adiabatic force at t_3 (see Fig.1(a)), namely

$$F_1^{i\alpha}(t) = -\frac{\partial V_1}{\partial R_{i\alpha}(t)} = \frac{-1}{R_{i\alpha}(t_3) - R_{i\alpha}(t_1)} \left[\frac{\partial U_-}{\partial R_{i\alpha}(t_3)} (R_{i\alpha}(t) - R_{i\alpha}(t_1)) - \frac{\partial U_+}{\partial R_{i\alpha}(t_1)} (R_{i\alpha}(t) - R_{i\alpha}(t_3)) \right] \quad (7)$$

and

$$F_2^{i\alpha}(t) = -\frac{\partial V_2}{\partial R_{i\alpha}(t)} = \frac{-1}{R_{i\alpha}(t_3) - R_{i\alpha}(t_1)} \left[\frac{\partial U_+}{\partial R_{i\alpha}(t_3)} (R_{i\alpha}(t) - R_{i\alpha}(t_1)) - \frac{\partial U_-}{\partial R_{i\alpha}(t_1)} (R_{i\alpha}(t) - R_{i\alpha}(t_3)) \right] \quad (8)$$

for $t_1 \leq t \leq t_3$, in which U_+ and U_- are adiabatic potential energy surfaces, respectively along a trajectory. Diabatic coupling in Eq. (2) is generalized by $2V_{12}(t) = U_+(t) - U_-(t)$. Finally we get two effective parameters in Eqs. (1) and (2) at time $t = t_2$ along a trajectory based on only two adiabatic potential energy surfaces and its gradients. It should be noticed that the integration time step should be small enough to keep good linear approximation of potential energy surfaces in order to have accurate diabatic forces in Eqs. (7) and (8). The present fitting scheme of the diabatic forces is consistent with the velocity-Verlet method for on-the-fly trajectory calculation in which the forces within the integration time step are considered as constant approximately. Once the time step is small enough to converge calculation for on-the-fly trajectory, it converges multidimensional diabatic forces in Eqs. (7) and (8). There is no additional time step requirement for nonadiabatic transitions. This is different from applying TFS switching probability in which the time step for computing accurate nonadiabatic transitions is much smaller than the time step for computing accurate velocity-Verlet trajectory.

Another question is how to define trajectory hopping direction for classical nuclear moment. Actually nonadiabatic coupling term $\sum_{i=1}^N \dot{\mathbf{R}}_i \cdot \mathbf{d}_{12}^i$ indicates that hopping direction should be in the direction of nonadiabatic coupling vector because this direction has maximum nonadiabatic transition probability. Following this idea, we define a self-consistent hopping direction by the following vector,

$$s_{i\alpha} = \frac{F_2^{i\alpha} - F_1^{i\alpha}}{\sqrt{m_i}} \quad (9)$$

with normalized vector as

$$\mathbf{n}_i = \frac{1}{\sqrt{s_{ix}^2 + s_{iy}^2 + s_{iz}^2}} (s_{ix}, s_{iy}, s_{iz}). \quad (10)$$

Analytical switching probability in Eq. (3) increases with product of the two parameters defined in Eqs. (1) and (2) as,

$$a^2 b^2 \propto \frac{1}{\mu} \frac{(F_2 - F_1)^2}{(V_{12})^4} = \sum_{i=1}^N \frac{1}{m_i} \sum_{\alpha=x,y,z} \frac{(F_2^{i\alpha} - F_1^{i\alpha})^2}{(V_{12})^4} \geq \sum_{i=1}^N \frac{1}{m_i} \sum_{\alpha=x,y,z} \left[\frac{((F_2^{i\alpha} - F_1^{i\alpha}) \mathbf{n}'_{i\alpha})}{V_{12}^2} \right]^2 \quad (11)$$

in which \mathbf{n}'_i is unit vector in arbitrary direction, only $\mathbf{n}'_i = \mathbf{n}_i$ leads to the maximum $a^2 b^2$ and in turn it leads to the maximum nonadiabatic transition probability and this can be seen from Landau-Zener formula for one passage nonadiabatic transition given by

$$p = \exp\left[-\frac{\pi}{4\sqrt{a^2 b^2}}\right] = \exp\left[-\sqrt{\frac{2\mu\pi^2}{\hbar^2(E_t - E_x)}} \frac{(V_{12})^2}{|F_2 - F_1|}\right]. \quad (12)$$

This switching probability depends on a ratio between adiabatic potential energy gap and force difference at the avoided crossing. It should be emphasized that hopping direction defined in Eq. (10) is not necessary to be direction of nonadiabatic coupling vector. In principle, the regularized states introduced by Köppel *et al.* [25] can provide the hopping direction (see Eq. (A.8) in Appendix A). However, we propose a simple algorithm for the hopping direction in which the nonadiabatic switching probability has the maximum at the avoided crossing. .

Final task is to set up relation for classical momentum before and after hopping. We could decompose momentum into parallel and perpendicular direction with respect to hopping direction vector \mathbf{n}_i (see Fig.1(b))

$$\mathbf{P}_{i//} = (\mathbf{P}_i \cdot \mathbf{n}_i) \mathbf{n}_i \quad \text{and} \quad \mathbf{P}_{i\perp} = \mathbf{P}_i - (\mathbf{P}_i \cdot \mathbf{n}_i) \mathbf{n}_i. \quad (13)$$

Momentum component $\mathbf{P}_{i\perp}$ is unchanged before and after hopping and energy conservation provides another relation for momentum component $\mathbf{P}_{i//}$, namely

$$\mathbf{P}_{i\perp}(+,t) = \mathbf{P}_{i\perp}(-,t) \quad (14)$$

and

$$E_t = U_+(t) + \sum_{i=1}^N \frac{\mathbf{P}_{i//}^2(+,t)}{2m_i} = U_-(t) + \sum_{i=1}^N \frac{\mathbf{P}_{i//}^2(-,t)}{2m_i} \quad (15)$$

in which $(+,t)$ and $(-,t)$ stand for momentum component on upper and lower adiabatic potential energy surfaces, respectively at time t . The last assumption assumes that parallel component of momentum keeps direction unchanged before and after hopping, and then simple scaling factor can be obtained from Eq. (15) to determine magnitude change of parallel component of momentum.

Along an on-the-fly running trajectory, we first determine the minimum potential energy gap at an avoided crossing and then compute the effective coupling parameter a^2 in Eq. (1), if a^2 is larger than 1000, the switching probability is set up to unity (diabatic limit) and if a^2 is smaller than 0.001, the switching probability is set up to zero (adiabatic limit). When $1000 > a^2 > 0.001$, calculation of an attempted hopping with switching probability is actually performed and it is possible to have multiple hops along a single trajectory. However, in practical simulation the larger switching probability, the larger momentum component along the hopping direction that is perpendicular to the seam line, and thus the trajectory usually moves away from the seam at avoided crossings where hopping is taken place. This has been observed in the present simulation of photoisomerization in azobenzene in which few trajectories experience multiple back-and-forth switches among a thousand sampling

trajectories. Now we complete the present new formalism for nonadiabatic molecular dynamics based on only two adiabatic potential energy surfaces and its gradients along a trajectory in the case of avoided crossing type of nonadiabatic transitions.

3. Application to photoisomerization in azobenzene

The analytical switching probability in global approach is applied to an on-the-fly surface hopping trajectory for photoisomerization in azobenzene and potential energy surfaces and its gradients are calculated by ab initio quantum chemistry method at SA2-CAS(6,6)/6-31G level with the Molpro 2009.1 program package [26].

3.1. Comparison with various CASSCF calculations.

Number of average states, number of active electrons and number of active orbitals in CASSCF method are actually correlated and various combinations of them should be tested to determine an affordable choice at CASSCF level for dynamic simulation without losing accuracy for potential energy surfaces. Table 1 presents vertical excitation energies calculated from various SAN-CAS(n,m) methods. The multireference perturbation configuration method (CIPSI) [27] shows the best results in comparison with experimental values [28]. Among all CASSCF methods, SA2-CAS(6,6)/6-31G performs best. If we include S_2 state, the present SA3-CAS(6,6)/6-31G shows pretty large vertical excitation energies just like one performed by SA3-CAS(10, 8)/6-31G*/6-31G level [19]. The values listed in Table 1 are obtained with three singlet states plus one triplet state in calculation. The present SA4-CAS(6,6)/6-31G calculation shows slightly worse results in comparing with SA2-CAS(6,6)/6-31G level, and thus it is not necessary to include more averaged-state at CAS(6,6)/6-31G level. We have done calculation for vertical excitation energies with SA5-CAS(6,4)/6-31G in order to compare with

calculation by SA5-CAS(6, 4)/STO-3G [16] that presents quantum yields and lifetimes for photoisomerization from both cis- and trans-azobenzene. Actually the SA2-CAS(14, 12)/6-31G* calculation produces not good vertical excitation energies [29], and this is evidence that more active space and more active electrons do not perform better than less active space and less active electrons. Finally, we decide to use SA2-CAS(6,6)/6-31G level to perform the present nonadiabatic molecular dynamics simulations.

3.2. Geometry optimizations and energy profiles.

Within ab initio quantum chemistry method at SA2-CAS(6,6)/6-31G level, we found optimized geometries of cis- and trans-azobenzene in both S_0 and S_1 states, three transition states in S_0 state and one transition state in S_1 state, and two conical intersections between S_0 and S_1 states. Atom numbering is given in Fig.2. Table 2 summarizes important internal coordinates around conical intersections; NN and two CN bond lengths, two NNC bond angles, CNNC and two NNCC dihedral angles for optimized geometries and energies. Optimized geometries of cis- and trans-azobenzene in S_0 state agree well with experiment results [28, 30, 31], and we obtained optimized geometries for cis- and trans-azobenzene in S_1 state as well. Calculated vertical excitation energies 3.05eV(cis) and 2.99eV(trans) are also in good agreement with the experimental values 2.92eV(cis) and 2.82eV(trans). We found three transition states in S_0 state which are possible pathways for isomerization in azobenzene, namely rotation (TS-rot), planar inversion (TS-planar-inv) and the inversion-assisted rotation (TS-inv-rot). We found one transition state corresponding to the rotation pathway (TS-rot) in S_1 state. We found two conical intersections between S_0 and S_1 states, namely CI-rot and CI-inv. Energy of CI-inv is 0.42eV higher than energy of CI-rot and even 0.29eV higher than energy of trans-azobenzene in S_1 state as shown in the second column of Table 2. This is partly explained why CI-inv is not accessible for dynamic simulation starting from S_1 state. Full

geometry informations in Cartesian coordinates for Table 2 are given in Supporting Information.

Figure 3 plots energy profiles along intrinsic reaction coordinate (IRC) based on three transition states TS-rot, TS-planar-inv, and TS-inv-rot in S_0 state. The energy of TS-inv-rot is the lowest one and its structure shows that the two benzene rings are perpendicular to each other. Potential energy curve along IRC in S_1 state shows a barrier in the trans side and has rather flat region in cis side as shown in Fig. 3(a). The geometry of TS-inv-rot is far from the geometry of two conical intersections and thus this pathway is unfavorable for photoisomerization in S_1 state. Although the energy of TS-rot is 0.19 eV higher than the TS-inv-rot in S_0 state, it shows small energy gap between S_0 and S_1 states and its geometry is close to CI-rot geometry as shown in Fig. 3(b). Therefore, TS-rot is most favorable pathway for photoisomerization in S_1 state. The energy of TS-planar-inv is quite high in S_0 state, and its geometry is far from both geometries of conical intersections. Besides, the isomerization follows this path in S_1 state is hindered by the large barrier of more than 1.1 eV. This explains why we see only TS-rot pathway for photoisomerization in dynamic simulation. We have scanned the two-dimensional potential energy surfaces near vicinity of the two conical intersections as shown in Fig.S3 of Supporting Information.

3.3. Setting up initial and final conditions for trajectory simulation

A canonical ensemble with temperature $T = 300\text{K}$ is used to specify initial conditions of trajectories. We first do frequency calculation at cis- azobenzene and trans-azobenzene in S_0 state, where we set up normal-mode velocities with randomly choice of plus or minus sign and then convert them back to velocities in Cartesian coordinates. Prepared initial coordinates and velocities in Cartesian coordinates at cis-azobenzene and trans-azobenzene in S_0 state are vertically excited to S_1 state in Franck-Condon region where trajectory starts evolution. Test

runs with time step 0.1fs, 0.25fs, 0.5fs, 0.75fs, and 1fs are performed to check robustness of two parameters defined in Eqs. (1) and (2), and then we select 0.5fs time step from beginning to end of entire dynamic simulation for trajectory.

The Monte Carlo method is employed to calculate quantum yield with equal weight to all trajectories. Thus, quantum yield is equal to N_r/N where N is total number of trajectories and N_r is number of reactive trajectories with standard error $\sqrt{(N - N_r)/(NN_r)}$. In total, 800 trajectories have been run starting from cis-azobenzene up to 200 fs (trajectories are accounted as resonance if they still in S_1 state beyond 200fs), while 600 trajectories have been run starting from trans-azobenzene up to 1.5ps (trajectories are accounted as resonance if they still in S_1 state beyond 1.5ps without experience of an attempted hopping, otherwise extended to 2.0ps). There are about twenty percent resonance trajectories starting from trans-azobenzene, and this is because there is deep potential well around Franck-Condon region in S_1 state and trajectories can be trapped there for a long time. On the contrary, there is no resonance trajectory starting from cis-azobenzene because there is very shallow potential well in Franck-Condon region of S_1 state and trajectories go down to conical intersection very fast.

The isomerization lifetime is estimated by calculating average population decay in S_1 state with respect to time evolution and then fitting this decay curve to exponential function $f(t) = \exp[-(t - t_d)/\tau]$, where t_d is the onset time of the S_1 population loss and τ is the time constant for the exponential decay. The lifetime is estimated as the value of $\tau + t_d$. The error bar of the lifetime is estimated from fitting procedure. When number of sampling trajectory is small, the decay curve is not smooth and exhibits zigzag feature. By fitting upper and lower bound of this zigzag curve, we obtain error estimation of the lifetime. When the decay curve is getting smooth with respect increasing sampling trajectories, this error becomes small.

4. Results and discussion

Table 3 shows simulated quantum yields and lifetimes for both cis-to-trans and trans-to-cis photoisomerization in comparison with the other recent results simulated by the TFS switching probability, the energy gap depended empirical switching probability, and experimental measurements. The present simulated results are in good agreement with the other previous simulations and experiment values in some extend. Simulated quantum yield and lifetime of cis-to-trans (trans-to-cis) converge to 0.39 and 53fs (0.33 and 0.81ps) with 800 (600) sampling trajectories as shown in Table 3.

For quantum yield and lifetime of cis-to-trans, the present results 0.46 and 54fs up to 50 sampling trajectories agree with the previous results 0.45 and 60fs (200 sampling trajectories) simulated by SA5-CAS(6,4)/STO-3G with the TFS switching probability [16]. For trans-to-cis case, the present results 0.30 and 1.0ps up to 20 sampling trajectories agree with their results 0.28 and 1.86ps (100 sampling trajectories). It is evidently that the present simulation with analytical switching probability is in fast convergence in comparison with those simulated by TFS switching probability. Actually, there are two factors to determine convergence of nonadiabatic process; one is number of sampling trajectory on a single adiabatic potential energy surface and the other is number of sampling trajectory to simulate nonadiabatic switching probability between two adiabatic potential energy surfaces. Let us go back to Tully's original paper [3] in which the TFS switching probability is originated with one-dimensional two-state model systems in which convergence is only depending on number of trajectories between two potential energy curves; the smaller switching probability along evolution of trajectory is, the more sampling trajectories are required to converge overall nonadiabatic transition. The TFS switching probability stands for local nonadiabatic transitions

and hopping could happen anywhere along one-dimensional two-state potential energy curves, while the present analytical switching probability stands for global nonadiabatic transition and hopping could happen only at avoided crossing. Therefore the present method converges faster than TFS method along this one-dimensional two-state potential energy curves. However, if a conical intersection has the non-avoided crossing seam or avoided crossing with higher order than linear dependence of coordinates with respect to adiabatic potential energy surfaces, the present global approach cannot take into account these nonadiabatic transition regions while the local approach can.

Figure 4 shows distribution of successful hopping points with respect to CNNC dihedral angle; the present CNNC dihedral angle is distributed in the range $[-95^\circ, -80^\circ]$ (see Fig.4(a)) in comparison with $[-100^\circ, -70^\circ]$ from Ref.16 for cis-to-trans isomerization and is distributed in the range $[-105^\circ, -80^\circ]$ (see Fig.4(b)) in comparison with $[-160^\circ, -80^\circ]$ from Ref.16 for trans-to-cis isomerization. Both the present and their calculations share the common feature in which the successful hopping points are taken place mostly in the range of CNNC dihedral angle larger (smaller) than -92.6° at conical intersection for cis-to-trans (trans-to-cis) isomerization. However, their distributions are very sparse in wide region of CNNC dihedral angle around conical intersection, especially in trans-to-cis case. This is because that trajectory takes much long time to reach conical point for trans-to-cis case, so that hopping points can be everywhere driven by the TFS switching probability and many successful hopping points can be taken place with small TFS switching probability. That means much more sampling trajectories are needed to converge their calculation for trans-to-cis isomerization. Their simulations with fixed all CH bonds somehow helps convergence with less number of trajectories, otherwise distribution of the successful hopping points can get even sparse. This is

exactly case for simulation with full degree of freedom at SA3-CAS(8,6)/6-31G level [19] that presents quantum yield 0.65 and lifetime 67fs with up to 70 sampling trajectories for cis-to-trans isomerization. In general, many hopping trajectories can occur with very small TFS switching probability if trajectories take long time to reach conical intersection zone, and then convergent overall nonadiabatic transition must require huge number of sampling trajectories. The hopping spots in terms of the CNNC dihedral angle are taken place within 15° (25°) interval by the present global approach in comparison with 30° (80°) interval by the local approach from Ref.16 for cis-to-trans (trans-to-cis) photoisomerization. In the case of cis-to-trans, the isomerization dynamics is in short time so that lifetime is 60fs with 200 sampling trajectories in the local approach and it is 53fs with 800 sampling trajectories in the global approach in comparison with experiment results of 70 ~100fs. The two approaches agree well each other. On the other hand, in the case of trans-to-cis, the isomerization dynamics is in long time so that lifetime is 1.86ps with 100 sampling trajectories in the local approach and it is 0.81ps with 600 sampling trajectories in the global approach in comparison with experiment results of 0.9~1.4ps. It seems that the local approach is in one end, but the global approach in another. The narrow window of the surface hopping spots in the present global approach directly leads to the short lifetime. Actually, this can be also seen from the force field simulation in which lifetime is 0.44ps with 1500 sampling trajectories in terms of semiempirical energy-gap switching probability [21], and that the effective the surface hopping spots is even narrower than the present global approach due to the energy gap in conical intersection being far apart quickly in terms of the CNNC dihedral angle. However, three approaches present the similar results for the quantum yield; it is 0.28, 0.33, and 0.52 in the local, global and energy-gap approaches, respectively for trans-to-cis isomerization. In conclusion, the lifetime is more

sensitive than the quantum yield in terms of the spots of trajectory hopping distribution. The present global approach can avoid small hopping events results in fast convergence in one hand, but in another hand it may neglect the certain region where nonadiabatic transitions could accumulate in long time dynamics. Hopping distribution in energy is around 0 to 0.25 eV (see the first panel of Fig.4(a)) in cis-to-trans case while around 0 to 0.2eV in trans-to-cis case. However, hopping distribution in effective coupling parameter a^2 and effective collision energy b^2 are all in region of $a^2 \sim [0.1, 10^5]$ (see second panel of Fig.4(a, b)) and $b^2 \sim [1, 100]$ (see third panel of Fig.4(a, b)) for both cis-to-trans and trans-to-cis cases. The present analytical switching probability that represents global nonadiabatic transitions at conical intersection zone (avoided crossing zone) is determined by distribution of these two dimensionless parameters and trajectories serve as simulator to decode the distribution of switching probabilities.

Table 4 shows that average hopping time starting from cis-isomer is 55fs (50fs) for reactive (non-reactive) counterclockwise trajectories which are in good agreement with 64fs (58fs) reported from Ref.16. The present average velocity of CNNC angle at hopping spots is about -1.80 deg/fs (1.39 deg/fs) for reactive (non-reactive) counterclockwise rotation trajectories in comparison with -2.56 deg/fs (0.33 deg/fs) reported from Ref.16. This difference may come from different initial conditions since we do not observe clockwise rotation starting from cis-isomer. This is understandable from analysis of initial condition that can control rotation of trajectory [19]. The present average energy gap at hopping spots is about 0.08eV starting from cis-isomer, while it is about 0.05eV starting from trans-isomer. This reflects that potential energy surface around conical intersection is not isotropic. Actually starting from trans-isomer, we do observe both clockwise and counterclockwise rotation for reactive and

nonreactive trajectories as shown in Table 4. This is because that trans-isomer is almost planar geometry. Average hopping time at hopping spots from trans-isomer is about 637fs which is shorter than 800fs reported from Ref.16. The trajectories starting from trans-isomer need several hundred femtosecond to leave the Franck-Condon region, and that leads long average hopping time and lifetime. On the other hand, the trajectories starting from cis-isomer need several tenth femtosecond to leave the Franck-Condon region and then go fast toward conical intersection, and this leads to short average hopping time and lifetime.

There are five most important angles involving motion of photoisomerization; the two NNC bond angles, the two NNCC and one CNNC dihedral angles, and we plot several typical trajectories in Fig.5 and Fig.6 to show how these five angles evolves with time along trajectory. A reactive (non-reactive) trajectory starting from cis-isomer takes about 60fs (50fs) to hop down S_0 state with effective coupling and collision energy parameters $a^2 = 14.79$ and $b^2 = 3.52$ ($a^2 = 75.35$ and $b^2 = 4.82$) at the hopping point as shown in left (right) panel of Fig.5. In both reactive and non-reactive cases, the CNNC dihedral angles show the most rapidly changing, and this indicates that the rotation pathway dominates the isomerization process. The NNCC dihedral angles change in the opposite direction compare to the CNNC dihedral angle. The two NNC bond angles vibrates slowly until reaching conical point, one of NNC bond angles increase to about 135° - 140° while the other stays around 115° , close to optimized CI-rot structure of 140.6° and 121.8° , respectively. After hopping, the two NNC angles move in opposite direction for both reactive and non-reactive trajectories. Potential energy gap between S_0 and S_1 along both reactive and non-reactive trajectories are rapidly decreasing down to the conical point, and then the energy gap is rapidly far apart toward the product region. This is indication of fast isomerization motion for trajectory starting from cis-isomer. On the other

hand, the trans-azobenzene has a planar symmetric structure, and thus the trajectories have almost equal opportunity to follow the clockwise and counterclockwise rotation pathways. A clockwise (counterclockwise) reactive trajectory starting from trans-isomer takes about 800fs (850fs) to hop down S_0 state with effective coupling and collision energy parameters $a^2 = 0.22$ and $b^2 = 1.95$ ($a^2 = 35.84$ and $b^2 = 4.26$) at the hopping point as shown in left (right) panel of Fig.6(a). A clockwise (counterclockwise) non-reactive trajectory starting from trans-isomer takes about 580fs (430fs) to hop down S_0 state with effective coupling and collision energy parameters $a^2 = 9.50$ and $b^2 = 3.07$ ($a^2 = 48.17$ and $b^2 = 6.65$) at the hopping point as shown in left (right) panel of Fig.6(b). The isomerization process from trans-isomer is much slower than that from cis-isomer. Except the CNNC dihedral angle, the other four angles fluctuate around their initial values along trajectories. The CNNC dihedral change slowly vibrates around approaching to the conical region with CNNC dihedral angle ($\sim \pm 90^\circ$). In hopping region, the NNCC dihedral angles move in opposite direction with respect to the CNNC dihedral angle. The two NNC bond angles separate in the conical region with one of them increases to about 140° while the other decreases to around 120° . We show one typical resonance trajectory in Fig.S1 of Supporting Information where all five angles vibrate around the initial structure independently and they never pass through the conical region. We have done more time propagation up to 3ps for those resonance trajectories, and they still vibrate on S_1 potential energy surface. It may need more and more time to bring them down.

We plot population decay from S_1 state in Figure 7. Figure 7(a) shows only one time scale decay from cis-isomer as observed in Ref.16. Figure 7(b) shows that population decay from trans-isomer has fast decay component around 350-450fs and slow decay component after 450fs in S_1 state, and these two-time-scale decays are also observed by SA5-CAS(6,4)/STO-3G simulation [16]. We fitted fast and slow motion to exponential function

separately and then average them to have final life time in Table 3.

5. Concluding remarks

By generalizing the two unitless parameters (effective coupling constant and effective collision energy) originally for avoided crossing type of nonadiabatic transitions in diatomic molecule to many-atom molecule, we have accomplished the new algorithm to calculate switching probability on-the-fly along trajectory based on only two adiabatic potential energy surfaces and its gradients. Method is simple and accurate for applying in the case of localized nonadiabatic transitions induced by conical intersections. Simply speaking, if one can do trajectory based molecular dynamics on a single electronic adiabatic potential energy surface, one can do trajectory based non-Born-Oppenheimer molecular dynamics on excited electronic adiabatic potential energy surfaces. This is also potentially useful for force field excited-state molecular dynamic simulation and it requires force fields only for electronic adiabatic potential energy surfaces.

Incorporating with on-the-fly trajectory surface hopping algorithm, we have applied the present new method to compute analytical switching probability and then to simulate azobenzene photoisomerization for both cis-to-trans (800 sampling trajectories) and trans-to-cis (600 sampling trajectories) at the SA2-CASSCF (6, 6)/6-31G quantum chemistry level. Extensive comparison has been made with the previous simulations performed by Tully's fewest switching method. Quantum yield and lifetime simulated with the present method basically agree with those simulated with TFS method. Average surface hopping time from cis-somer (trans-isomer) is about 53fs (637fs) simulated from the present method in comparison with 50fs (800fs) simulated by TFS method. The present method needs less number of sampling trajectories to converge overall nonadiabatic switching probability than those from

TFS method. However, the present method takes account narrower region of nonadiabatic transition zones than TFS method, and it may results in the certain inaccuracy for more detailed mechanistic aspects like state-to-state molecular dynamics.

The present method can keep the same time step for computing both accurate velocity-Verlet trajectory and accurate nonadiabatic transitions, while in the TFS switching method time step for computing accurate nonadiabatic transitions is much smaller than time step for computing accurate velocity-Verlet trajectory.

The TFS switching method can deal with not only avoided crossing type of nonadiabatic transitions, but also non-avoided crossing type of transitions. In general, there are three independent quantities at nonadiabatic transition zone; two adiabatic potential energy surfaces and one nonadiabatic coupling. In the present method, we need only two adiabatic potential energy surfaces and this is due to avoided crossing type of nonadiabatic transition in which Landau-Zener type of switching probability includes contribution of nonadiabatic coupling already. In general, we need the rotation angle to transform potential energy surfaces from adiabatic representation to diabatic representation, and this rotation angle $\theta(R)$ is in range of zero to $\pi/4$ degree in which $\theta(R) = \pi/4$ represents maximal mixing of the two representations regarded as Landau-Zener type of nonadiabatic transitions [32]. Analytical switching probability including this rotation angle is formulated for general two-state nonadiabatic transition (including both avoided and non-avoided types of nonadiabatic transitions) [33]. It is very challenge task to generalize this rotation angle in general along on-the-fly trajectory without calculating nonadiabatic coupling. The present study is focusing on avoided crossing types of nonadiabatic transitions and it is demonstrated to work well for conical intersection type of nonadiabatic transitions in azobenzene photoisomerizations. We will report the other

simulations of photoisomerizations with two or more excited states calculated by ab initio quantum chemistry method associated with the present global approach of switching probability in the near future.

Acknowledgements

This work is supported by Ministry of Science and Technology of the Republic of China under grant nos. 100-2113-M-009-005-MY3 and 103-2113-M-009 -007 -MY3. L. Y. thanks support from Postdoctoral Fellowship by Ministry of Science and Technology of the Republic of China under grant nos. 102-2811-M-009 -044 and 103-2811-M-009 -048. C. X. thanks support from visiting student fellowship by National Chiao Tung University. C. Z. thanks the MOE-ATU project of the National Chiao Tung University for support.

Appendix A: convert multidimensional conical intersection to one-dimensional avoided crossing along a trajectory

It is known at the crossing point of a conical intersection that the nonadiabatic coupling vector has a removable singularity with a pole of the order 1 and thus well behavior function of electronic diabatic potential energy surfaces can be defined. Following the regularized diabatic states introduced by Köppel *et al.* [25], the diabatic potential energy surfaces can be written in the following form:

$$\mathbf{W}_{reg} = \begin{pmatrix} \frac{U_+ + U_-}{2} & 0 \\ 0 & \frac{U_+ + U_-}{2} \end{pmatrix} + \begin{pmatrix} \sum_{i=1}^N \kappa_i Q_i & \sum_{j=1}^M \lambda_j Q_j \\ \sum_{j=1}^M \lambda_j Q_j & -\sum_{i=1}^N \kappa_i Q_i \end{pmatrix}, \quad (\text{A.1})$$

where U_+ and U_- are upper and lower *ab initio* adiabatic potential energy surfaces, respectively, and the coupling terms are given by

$$\kappa_i = \frac{1}{2} \left(\frac{\partial U_+}{\partial Q_i} - \frac{\partial U_-}{\partial Q_i} \right) \Bigg|_{\mathbf{Q}=0} \quad \text{and} \quad \lambda_j = \frac{1}{2} \left(\frac{\partial U_+}{\partial Q_j} - \frac{\partial U_-}{\partial Q_j} \right) \Bigg|_{\mathbf{Q}=0}, \quad (\text{A.2})$$

where the crossing point is assumed at multidimensional coordinates $Q_1=Q_2=\dots=0$ ($\mathbf{Q}=0$) and Eq. (A.1) is valid in the neighborhood of the crossing point. Now, we can compute gap two adiabatic potential energy surfaces as

$$\Delta V = \sqrt{\left(2 \sum_{i=1}^N \kappa_i Q_i \right)^2 + 4 \left(\sum_{j=1}^M \lambda_j Q_j \right)^2}. \quad (\text{A.3})$$

Assume that a multidimensional trajectory can be expressed in terms of a one-dimensional curved coordinate s , and thus we have $Q_i=Q_i(s)$. It is the trajectory that passes through the crossing region and reaches the point $s_0 = s(t_0)$ at time t_0 where the potential gap is the minimum. We expand coordinate Q_i around s_0 as

$$Q_i(s) = Q_i(s_0) + \left. \frac{dQ_i}{ds} \right|_{s=s_0} (s - s_0). \quad (\text{A.4})$$

Inserting Eq. (A.4) into Eq. (A.3) leads to

$$\Delta V = \sqrt{(F_1 - F_2)^2 (s - s_0)^2 + 4(V_{12})^2} \quad (\text{A.5})$$

in which (at $s = s_0$, the gap is minimum so that the term with $(s - s_0)$ vanishes in Eq. (A.5))

$$(F_2 - F_1)^2 = 4 \sum_{i,\alpha=1}^N \kappa_i \kappa_\alpha \left(\frac{dQ_i}{ds} \right)_{s_0} \left(\frac{dQ_\alpha}{ds} \right)_{s_0} + 4 \sum_{j,\beta=1}^M \lambda_j \lambda_\beta \left(\frac{dQ_j}{ds} \right)_{s_0} \left(\frac{dQ_\beta}{ds} \right)_{s_0} \quad (\text{A.6})$$

and

$$(V_{12})^2 = \sum_{i,\alpha=1}^N \kappa_i \kappa_\alpha Q_i(s_0) Q_\alpha(s_0) + \sum_{j,\beta=1}^M \lambda_j \lambda_\beta Q_j(s_0) Q_\beta(s_0). \quad (\text{A.7})$$

By introducing coordinate transformation $Q_i \rightarrow Q'_i$, we finally reach

$$(F_2 - F_1)^2 = 4 \sum_{i=1}^N \kappa_i'^2 \left(\frac{dQ'_i}{ds} \right)_{s_0}^2 + 4 \sum_{j=1}^M \lambda_j'^2 \left(\frac{dQ'_j}{ds} \right)_{s_0}^2 \rightarrow \sum_{l=1}^{3n} [(F'_{2l} - F'_{1l}) n'_l]^2 \quad (\text{A.8})$$

and

$$(V_{12})^2 = \sum_{i=1}^N \kappa_i'^2 Q'_i(s_0)^2 + \sum_{j=1}^M \lambda_j'^2 Q'_j(s_0)^2 \rightarrow (V'_{12}(s_0))^2. \quad (\text{A.9})$$

Equation (A.5) shows one-dimensional two-state Landau-Zener avoided crossing along the curved coordinate and Eq. (A.8) is consistent with the present new algorithm Eq. (11) in the text. The hopping direction n'_l in Eq. (A.8) is selected as providing the maximum switching probability.

References

1. B. F. E. Curchod, U. Rothlisberger, and I. Tavernelli, *ChemPhysChem.*, 2013, **14**, 1314-1340.
2. D. Marx, and J. Hutter, *Ab Initio Molecular Dynamics: Basic Theory and Advanced Methods*, Cambridge University Press, Cambridge, 2009.
3. J. C. Tully, *J. Chem. Phys.*, 1990, **93**, 1061-1071.
4. N. L. Doltsinis, and D. Marx, *Phys. Rev. Lett.*, 2002, **88**, 166402.
5. C. F. Craig, W. R. Duncan, and O. V. Prezhdo, *Phys. Rev. Lett.*, 2005, **95**, 163001.
6. E. Tapavicza, I. Tavernelli, and U. Rothlisberger, *Phys. Rev. Lett.*, 2007, **98**, 023001.
7. M. S. Child, *Molecular Collision Theory* (Academic, London, New York, 1974).
8. C. Zhu, and H. Nakamura, *J. Chem. Phys.*, 1992, **97**, 8497-8514
9. C. Zhu, and H. Nakamura, *J. Chem. Phys.*, 1993, **98**, 6208-6222.
10. C. Zhu, H. Kamisaka, and H. Nakamura, *J. Chem. Phys.*, 2002, **116**, 3234-3247.
11. K.-L. Han, and B. Li, *J. Chem. Phys.*, 2008, **128**, 114116.
12. A.-H. Gao, B. Li, P.-Y. Zhang, and K.-L. Han, *J. Chem. Phys.*, 2012, **137**, 204305.
13. T. Ishida, S. Nanbu, and H. Nakamura, *J. Phys. Chem. A*, 2008, **113**, 4356-4366.
14. *Conical Intersections: Electronic Structure, Dynamics & Spectroscopy*. W. Domcke, D. R. Yarkony, and H. Köppel, Eds. World Scientific, Singapore, 2004.
15. C. Ciminelli, G. Granucci, and M. Persico, *Chem. Eur. J.*, 2004, **10**, 2327-2341.
16. Y. Ootani, K. Satoh, A. Nakayama, T. Noro, and T. Taketsugu, *J. Chem. Phys.*, 2009, **131**, 194306.
17. T. Cusati, G. Granucci, and M. Persico, *J. Am. Chem. Soc.*, 2011, **133**, 5109-5123.
18. O. Weingart, Z. Lan, A. Koslowski, and W. Thiel, *J. Phys. Chem. Lett.*, 2011, **2**, 1506-1509.

19. M. Pederzoli, J. Pittner, M. Barbatti, and H. Lischka, *J. Phys. Chem. A*, 2011, **115**, 11136-11143.
20. A. J. Neukirch, L. C. Shamberger, E. Abad, B. J. Haycock, H. Wang, J. Ortega, O. V. Prezhdo, and J. P. Lewis, *J. Chem. Theory Comput.*, 2014, **10**, 14-23.
21. G. Tiberio, L. Muccioli, R. Berardi, and C. Zannoni, *ChemPhysChem*, 2010, **11**, 1018 – 1028.
22. Y. Li and B. Hartke, *J. Chem. Phys.*, 2013, **139**, 224303.
23. H. M. Bandara, and S. C. Burdette, *Chem. Soc. Rev.*, 2012, **41**, 1809-1820.
24. L. Verlet, *Phys. Rev.*, 1967, **159**, 98-103.
25. H. Köppel, J. Gronki, and S. Mahapatra, *J. Chem. Phys.*, 2001, **115**, 2377-2388.
26. MOLPRO, a package of ab initio programs written by H.-J. Werner, and P. J. Knowles, version 2009.1, G. Knizia, F. R. Manby, M. Schütz, *et al.*
27. P. Cattaneo and M. Persico, *Phys. Chem. Chem. Phys.*, 1999, **1**, 4739-4743.
28. D. L. Beveridge and H. H. Jaffe, *J. Am. Chem. Soc.*, 1966, **88**, 1948-1953.
29. A. Cembran, F. Bernardi, M. Garavelli, L. Gagliardi, and G. Orlandi, *J. Am. Chem. Soc.*, 2004, **126**, 3234-3243.
30. J. A. Bouwstra, A. Schouten and J. Kroon, *Acta Cryst. C*, 1983, **39**, 1121-1123.
31. T. Tsuji, H. Takashima, H. Takeuchi, T. Egawa, and S. Konaka, *J. Phys. Chem. A*, 2001, **105**, 9347-9353.
32. C. Zhu, *Phys. Scr.* 2009, **80**, 048114.
33. C. Zhu, *J. Chem. Phys.* 1996, **105**, 4159-4172.

Table 1. Vertical excitation energies for cis- and trans-azobenzene. Various combinations of number of average states, active electrons and active orbitals are performed and compared in state-averaged CASSCF method.

Methods	cis-azobenzene (eV)	trans-azobenzene (eV)
SA2-CAS(6,6)/6-31G (this work)	3.05	2.99
SA2-CAS (14, 12)/6-31G* ^a	3.38	3.18
SA3-CAS(6,6)/6-31G (this work)	3.05	3.03
SA3-CAS (10, 8)/6-31G*/6-31G ^b	3.36	3.24
SA4-CAS(6,6)/6-31G (this work)	3.09	3.03
SA5-CAS(6,4)/6-31G (this work)	3.16	3.08
SA5-CAS (6, 4)/STO-3G ^c	3.78	2.96
CIPSI ^d	2.94	2.81
Expt ^e	2.92	2.82

^a Ref. 29, ^b Ref. 19, ^c Ref. 16, ^d Ref. 27: CIPSI calculation for 4 singlet and 2 triplet states, ^e Ref. 28.

Table 2. Optimized geometries and energies for equilibriums, transition states, and conical intersections in the ground state S_0 and the first singlet excited S_1 state. Energies are given in eV. Bond length r is given in angstrom (\AA) and bond angles a and dihedral angles d are given in degrees. E_{diff} is the energy gap between S_0 and S_1 states.

Geometry	Energy	E_{diff}	r_{NN}	r_{CN}	a_{NNC}	d_{CNNC}	d_{NNCC}
trans S_0	0.00	2.99	1.233	1.422/1.422	117.7/117.7	-180.0	-0.1/-0.1
Expt. ^a		2.82 ^b	1.260	1.427/1.427	113.6/113.6	180.0	0.0/0.0
Expt. ^c			1.247	1.428/1.428	113.9/113.9	180.0	0.0/0.0
cis S_0	0.78	3.05	1.231	1.435/1.435	125.9/125.8	-6.4	-52.7/-53.8
Expt. ^c		2.92 ^b	1.253	1.449/1.449	121.9/121.9	8.0	53.3/53.3
TS-inv-rot S_0	1.98	1.31	1.210	1.451/1.355	119.2/178.9	-8.5	-1.0/-103.4
TS-rot S_0	2.17	1.00	1.324	1.382/1.382	120.6/120.1	-85.5	-2.7/-2.6
TS-planar-inv S_0	2.21	1.17	1.228	1.447/1.383	121.5/177.1	0.0	0.0/0.0
cis S_1	3.29	1.01	1.213	1.376/1.376	149.2/148.9	0.0	0.0/0.0
trans S_1	2.53	1.95	1.245	1.383/1.383	130.7/130.7	-179.9	0.0/0.0
TS-rot S_1	2.53	0.51	1.244	1.404/1.391	125.5/133.5	-107.9	1.0/8.2
CI-rot S_0/S_1	2.42	0.00	1.244	1.413/1.372	121.8/140.6	-92.6	-0.2/2.7
CI-inv S_0/S_1	2.84	0.00	1.208	1.368/1.296	151.1/154.0	-180.0	0.0/0.0

^a Ref. 31, ^b Ref. 28, ^c Ref. 30.

Table 3. Convergence of simulated quantum yields and lifetimes for reactive photoisomerization $S_0 \leftarrow S_1$ in azobenzene with respect to the number of trajectories in comparison with selected simulation and experimental results.

	Number of trajectories	From cis-azobenzene		Form trans-azobenzene	
		Quantum yield	Lifetime (fs)	Quantum yield	Lifetime (ps)
SA2-CAS(6,6)	20	0.50±0.22	55.0±13.3	0.30±0.34	0.97±0.50
	50	0.46±0.15	53.6±8.6	0.30±0.22	1.00±0.30
	100	0.43±0.12	53.8±5.0	0.33±0.14	0.89±0.22
	150	0.43±0.09	53.1±5.0	0.32±0.12	0.88±0.20
	200	0.41±0.08	53.5±4.0	0.34±0.10	0.90±0.15
	300	0.40±0.07	53.4±4.0	0.34±0.08	0.82±0.10
	400	0.40±0.06	52.8±4.0	0.34±0.07	0.80±0.10
	500	0.40±0.06	52.6±4.0	0.34±0.06	0.82±0.10
	600	0.40±0.05	52.6±4.0	0.33±0.05	0.81±0.10
	800	0.39±0.04	53.1±3.0		
TDDFT ^a	400	0.58	121		
OM2/MRCI ^b	920	0.58	72		
SA3-CAS(10,8) ^c	70	0.65±0.11	67		
SA5-CAS(6,4) ^d	200/100	0.45	60	0.28±0.14	1.86
AM1 ^e	~200	0.61±0.03	50	0.33±0.03	0.35-0.41
FOCI-AM1 ^f	~600	0.49-0.58	70-135	0.24-0.37	0.39-0.54
Force field ^g	1500			0.16-0.52	0.44-5.3
Force field ^h	2000	0.59±0.08		0.11±0.03	
Expt ⁱ		0.41-0.56	100-170	0.23-0.35	0.9-1.4

^a Ref.20. ^b Ref.18 (lifetime is regarded as averaged hopping time). ^c Ref.19. ^d Ref.16 (CH bond constraints with RATTLE algorithms were implemented in simulation). ^e Ref.15. ^f Ref.17 (The solvent effects were represented by OPLS force field. The quantum yield and lifetimes were obtained by simulations in vacuum, *n*-hexane, methanol and ethylene glycol environments). ^g Ref. 21 (The quantum yield and lifetimes were obtained by simulations in vacuum, *n*-hexane, toluene, ethanol, anisole and ethylene glycol environments). ^h Ref.22, ⁱ Ref.23 and references therein.

Table 4. The averaged surface hopping time, averaged CNNC dihedral angle and its angle velocity and energy gap at hopping spots for trajectories started from cis- and trans-azobenzene.

	t_{hop} (fs)	d_{CNNC} (deg)	ω_{CNNC} (deg/fs) ^a	ΔE (eV)
cis reactive counterclockwise	55.3(64.0)	-86.1(-87.1)	-1.80(-2.56)	0.079
cis non-reactive counterclockwise	50.4(58.1)	-85.3(-87.0)	1.39(0.33)	0.082
trans reactive clockwise	641.5	-94.7	1.60	0.040
trans non-reactive clockwise	645.1	-96.8	0.85	0.050
trans reactive counterclockwise	598.0	94.3	-1.65	0.048
trans non-reactive counterclockwise	656.4	97.1	1.01	0.072

^a For the non-reactive trajectories the angle velocity is obtained as average of absolute value of angle velocity. Number in bracket are obtained from Ref.16.